

# Temperature field reconstruction method for aero engine exhaust using the colored background oriented Schlieren technology\*

SONG Fengcheng<sup>1</sup>, WU Jun<sup>1,2\*\*</sup>, ZHU Yuheng<sup>1</sup>, XU Haitao<sup>3</sup>, LI Yanling<sup>4</sup>, and YU Zhijing<sup>4</sup>

1. College of Aeronautical Engineering, Civil Aviation University of China, Tianjin 300300, China

2. State Key Laboratory of Precision Measuring Technology and Instruments, Tianjin University, Tianjin 300072, China

3. Xinjin Flight Training College, Civil Aviation Flight University of China, Guanghan 618300, China

4. College of Electronic Information and Automation, Civil Aviation University of China, Tianjin 300300, China

(Received 2 September 2021; Revised 20 October 2021)

©Tianjin University of Technology 2022

The detection of the jet temperature field in an aircraft engine tail is an effective way to reflect the running state of an engine. To solve the complicated detection process of current laser diagnostic methods, the colored background oriented Schlieren (CBOS) method was proposed to obtain a tail jet temperature field. First, the background Schlieren image with three-color points was collected for the exhaust gas temperature (EGT) field of the engine. Then the refractive index field of the engine exhaust was obtained according to the proposed CBOS method. Finally, the three-dimensional EGT field was reconstructed through the refractive index field. The simulation and the experimental results show the feasibility and effectiveness of the proposed method.

**Document code:** A **Article ID:** 1673-1905(2022)04-0243-8

**DOI** <https://doi.org/10.1007/s11801-022-1139-1>

As the core power unit in an aircraft, the aero-engine plays an important role in the aircraft system. It can improve the safety and economic efficiency of the aircraft by monitoring the status of the aero-engine. The temperature field of the exhaust gas from the aero-engine contains effective information such as the fuel's utilization ratio in the combustion chamber and the aging of the gas path. Therefore, the reconstruction for the temperature field of the exhaust gas is a useful method to monitor the status of the aero-engine. Most of the engine health monitoring (EHM) methods track the exhaust gas temperature (EGT) value in evaluating the health level of an engine<sup>[1,2]</sup>.

The measurement methods for the temperature field generally adopt contact temperature measurement and non-contact measurement. Contact temperature measurement is limited by space and it is not applicable to engine exhaust. Besides, contact temperature measurement is also easy to destroy the temperature field, for example, the probe temperature measures<sup>[3]</sup>.

Optical non-contact temperature measurement mainly includes fluorescence, lasers, and the Schlieren method. Among these measurement methods, fluorescence thermometry is not suitable for an engine due to the use of fluorescence materials<sup>[4]</sup>. Currently, tunable diode laser absorption spectroscopy (TDLAS) and its derivative

methods are widely used in combustion temperature field measurements. However, a set of test equipment of TDLAS can only obtain the temperature information along a single line. In order to reconstruct the three-dimensional temperature field, a great number of experimental equipments are needed.

Schlieren method has obvious advantages that can solve a large amount of flow field information. However, the traditional Schlieren method needs a great number of optical devices to build the optical path. Unlike the traditional Schlieren technique, the background-oriented Schlieren (BOS) technique is a non-contact detection method that employs cross-correlation image analysis for a temperature field. The background Schlieren technique proposed by MEIER et al<sup>[5]</sup> removes the precision lenses and cutting diaphragms used in the traditional Schlieren method so that the condition requirements of the measurement are reduced. VERSO et al<sup>[6]</sup> investigated the application of the BOS method in density field reconstruction. RAJSHEKHAR et al<sup>[7]</sup> analyzed the heat transfer process during the reconstruction of a temperature field with the traditional BOS method. SANGYOON et al<sup>[8]</sup> explored the use of the BOS method to reconstruct an engine tail flow field in a high temperature environment formed by an aero engine.

The BOS method in a high temperature region is

\* This work has been supported by the National Natural Science Foundation of China (No.52005500), the Basic Science-Research Funds of National University (No.3122019088), and the Foundation of Tianjin Educational Committee (No.2018KJ242).

\*\* E-mail: wujuncauc@163.com

affected by factors such as a large temperature gradient and the blurring of the background image. The traditional black-and-white speckle background Schlieren method has a lack of precision because in its high temperature gradient environment, image blur will be generated due to the different refractive indexes of light with different wavelengths, and the extraction offset will produce a large error. The colored background oriented Schlieren (CBOS) method is used to calculate a ray offset with different wavelengths.

The CBOS method, which replaced the black and white points in the BOS method with three-color points, has been used to reconstruct a 3D temperature field. Furthermore, using the target tracking method in the process of video inter-frame processing, the Kanade-Lucas-Tomasi (KLT) algorithm has been introduced for the matching of scattered spots in a background image. Based on the analysis of its feasibility, a speckle matching method using an improved KLT algorithm was proposed in this research in order to achieve the accurate and efficient matching of speckles. These two methods were applied to the reconstruction of an aero engine exhaust temperature field. The simulation of the aero engine exhaust was used to verify and compare the results of the aero engine exhaust temperature reconstruction.

The BOS method is based on the measurement of the deviation of light passing through a gaseous medium, expressed by the Gladstone-Dale formula as

$$n=1+G(\lambda)\rho, \tag{1}$$

where  $\rho$  is the gas density and  $G(\lambda)$  is the Gladstone-Dale constant, which is an attribute of gas. For the ideal constant pressure under constant pressure conditions, according to the Gladstone-Dale's equation formula, the relationship between the density and the temperature can be obtained via the simplification expressed as

$$T=\frac{\rho_0}{\rho}T_0=\frac{n_0-1}{n-1}T_0. \tag{2}$$

As shown in Fig.1,  $\Delta H$  represents the number of offset pixels produced by the same spot after the temperature field is added.  $\Delta H'$  is the spot offset corresponding to  $\Delta H$  in the actual background image. Based on this process, the offset corresponding to all of the spots can be obtained.

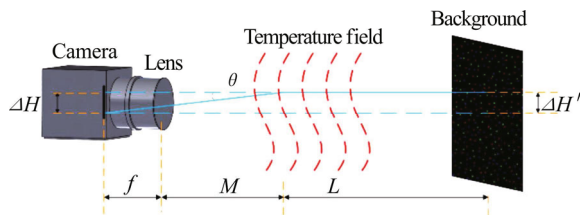


Fig.1 Schematic of the BOS method

Assuming that all of the records are paraxial rays and the deflection angle is extremely small, the deflection angles in the  $x$  and  $y$  directions can be calculated using

$$\theta_y = \frac{1}{n} \int_{\text{ray}} \frac{\delta n}{\delta y} dz, \tag{3}$$

$$\theta_y = (1 + M/L) \times \Delta H'_y / (L + M). \tag{4}$$

$\Delta H'_x$  and  $\Delta H'_y$  are the representative products of the image horizontal displacement offset  $\Delta H_x$ , the image vertical displacement offset  $\Delta H_y$ , and the camera resolution  $P$ , as follows<sup>[9]</sup>

$$\Delta H'_x = \Delta H_x \times P, \tag{5}$$

$$\Delta H'_y = \Delta H_y \times P. \tag{6}$$

Additionally, the relationship between the horizontal and vertical deflection angles of the light and the horizontal gradient of the refractive index and the vertical gradient of the refractive index can be determined from the formulas of the light deflection angles shown as

$$\theta_x = \frac{1}{n} \int_{\text{ray}} \frac{\delta n}{\delta x} dz, \tag{7}$$

$$\theta_y = \frac{1}{n} \int_{\text{ray}} \frac{\delta n}{\delta y} dz. \tag{8}$$

The CBOS method uses a computer to generate a large number of disordered scattered spots, in contrast to the black and white points used in the BOS method. These background points are placed in the background pattern, and these background points should cover 35%—70% of the background image.

As illustrated in Fig.2, all of the points are composed of red, green, and blue dots because the primary colors are red, green, and blue, which are easily captured by a color CCD camera. Various pure color points on the background image are evenly distributed at the same volume and proportion. The CCD camera used in this experiment is arranged by Bayer array, and the distortion of red, green and blue light obtained through the filter is minimal. The three channels of data obtained from the camera are these colors, and the background pattern chooses the spots of three colors randomly.

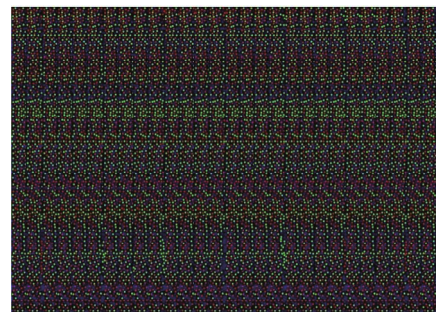


Fig.2 Background pattern

The processing procedure for a Schlieren image with the smear method for a colored background is as follows (see Fig.3). The first step is to take a picture of the background image. The second step is to divide the background image spot into the following parts: (1) pure red spots, (2) pure blue spots, (3) pure green spots, and (4)

all spots<sup>[10]</sup>. The third step is to use the particle image processing (PIV) method and then calculate the offset of all spots on the image. The fourth step is to obtain the offsets of the red, green, and blue points. The fifth step is to calculate whether the color scatter offset meets the standard deviation range  $\delta$  of the corresponding black and white offset. According to the references, the standard deviation range selected in this research was 0.36<sup>[11]</sup>. The sixth step is to calculate the offsets of all points and the offsets of three primary colors, and then calculate the average value of the correlation number. The seventh step is to determine the average offset of all positions by analyzing the results of the previous step. The eighth step is to reconstruct the density field by means of the calculated mean offset through the special form of the Radon transform Abel invert. The Abel transform formula is given by Eq.(9), for which  $I(x)$  is the density gradient for column symmetry and  $\varepsilon(r)$  is the radial distribution. The distribution radius is normalized to obtain the inverse transformation of the Abel, as shown in Eq.(10).

$$I(x) = \int_{-y_0}^{y_0} \varepsilon(r)dy, \tag{9}$$

$$\varepsilon(r) = -\frac{1}{\pi} \int_r^1 \frac{I'(x)}{\sqrt{x^2 - r^2}} dx, \quad (0 \leq r \leq 1). \tag{10}$$

Then the formulas are applied to the density field reconstruction yields, shown as follows

$$\varepsilon(r) = \frac{n(r)}{n_0} - 1, \tag{11}$$

$$\varepsilon(r) = -\frac{1}{\pi} \int_r^{R_0} \frac{I'_x(x)}{\sqrt{x^2 - r^2}} dx. \tag{12}$$

Finally, through the achieved density field, according to Eq.(2), the relationship between the density field and the temperature field is used to obtain the temperature field reconstruction.

In background image processing, the purpose of speckle matching is to establish the correspondence between speckles in different background images. However, in the actual measurement process, the matching process of speckles is sensitive to changes in camera position and illumination, which affects the measurement efficiency due to the inaccuracy in speckle identification and matching. In particular, for the reconstruction of an aero engine EGT field, the high-temperature and high-brightness environmental conditions have a higher impact on the speckle matching measurement. Generally, the traditional speckle matching methods are based on regional gray matching. The drawbacks of regional gray matching-based method are high time complexity and low calculation efficiency, especially when the measurement range is large. At the same time, because the speckle matching process for the background image shown above is very time consuming, the matching process is complicated. The feature-based matching method is widely used due to its advantages of fast matching speed, high matching accuracy, and strong

adaptability to light and noise.

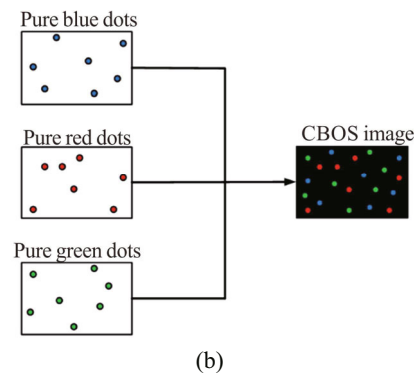
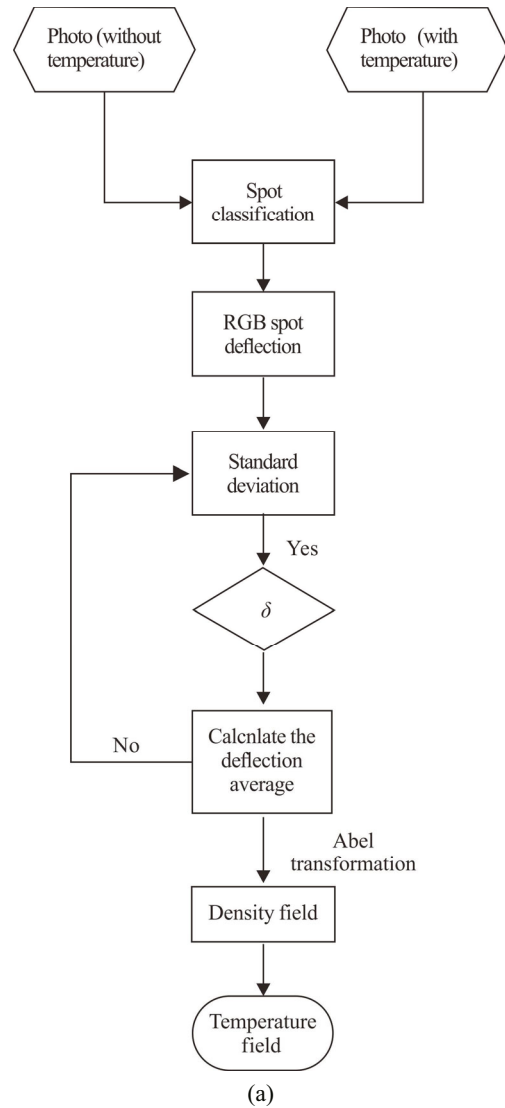


**Fig.3 (a) Illustration for CBOS; (b) Illustration for background pattern**

The matching process is mainly divided into the following two steps.

(1) Feature point extraction: LOWE et al proposed a local description of self-scale invariant feature transformation

(SIFT), which had invariance to scale transformation and rotation but also had a large amount of calculation data and high time complexity. RUBLEE et al<sup>[12]</sup> proposed a fast feature point extraction and description algorithm that optimized the operation speed on the basis of maintaining the invariance to scale transformation and rotation, but the detection effect of complex image feature points needed to be improved.

(2) Description and matching of feature points: To solve the existing problems of the basic matching method, SIFT, KE et al proposed the use of the principal component analysis (PCA) method to reduce the dimensionality of feature description data. However, without any prior knowledge, the PCA method increased the amount of calculation. DELPONTE et al<sup>[13]</sup> proposed the use of singular value decomposition to perform feature matching. However, the matching process was complex and it could not be used for wide baseline matching.

At present, the KLT algorithm is widely used in video processing procedures. The basic idea is to track the feature points in a video image by establishing constraint relationships at different moments. However, the application of the KLT algorithm in stereo matching for speckle measurement is still relatively limited. Therefore, the feasibility of the KLT algorithm needs to be analyzed. The algorithm is mainly based on the following three assumptions, constant brightness, continuous-time or motion being "tiny motion", and spatial consistency. To further analyze the feasibility of the KLT algorithm, a schematic diagram of the system was established, as shown in Fig.4.

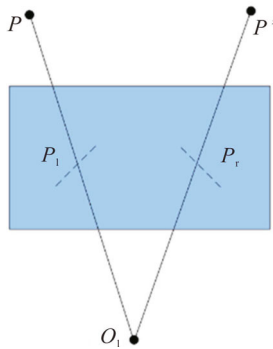


**Fig.4 Schematic diagram of the speckle matching system**

In the aero engine temperature field measurement system, the KLT algorithm in the video processing procedure can be applied to the speckle measurement stereo matching process, and the following perspective transformation expression can be obtained, shown as

$$\mathbf{x}' = (\mathbf{1} + \mathbf{D})\mathbf{x} + \mathbf{d},$$

$$\mathbf{D} = \begin{bmatrix} d_{xx} & d_{xy} \\ d_{yx} & d_{yy} \end{bmatrix}, \quad (13)$$

where  $\mathbf{D}$  is the deformation matrix,  $\mathbf{d}$  is the translation matrix at the center of the feature window, and  $\mathbf{x}'$  and  $\mathbf{x}$

represent the coordinates of the corresponding points of the two contrast images.

Therefore, based on the above research studies, by combining the grey distribution of one image and another image, the following expression can be obtained by setting the feature window and the optimization function, shown as

$$\varepsilon = \iint_w [J((\mathbf{1} + \mathbf{D})\mathbf{x} + \mathbf{d}) - I(\mathbf{x})]^2 \mathbf{w}(\mathbf{x})d\mathbf{x}, \quad (14)$$

where  $\mathbf{w}(\mathbf{x})$  expresses the weighting, which is the weighting function used to weight the target area to achieve a prominent effect for the key area. In addition, the change of the displacement  $\mathbf{d}$  of the feature window is a negligible amount compared to  $\mathbf{x}$ . Based on the above premises and assumptions, the following expressions can be achieved by processing the expansion and merger of similar items:

$$\begin{cases} \iint_w \mathbf{g}(\mathbf{g}^T \mathbf{u})\mathbf{w}(\mathbf{x})d\mathbf{x} = \iint_w [I(\mathbf{x}) - J(\mathbf{x})]\mathbf{g}\mathbf{w}(\mathbf{x})d\mathbf{x} \\ \iint_w \mathbf{g}\mathbf{x}^T(\mathbf{g}^T \mathbf{x})\mathbf{w}(\mathbf{x})d\mathbf{x} = \iint_w [I(\mathbf{x}) - J(\mathbf{x})]\mathbf{g}\mathbf{x}^T \mathbf{w}(\mathbf{x})d\mathbf{x} \end{cases}, \quad (15)$$

$$\begin{cases} \mathbf{u} = \mathbf{D}\mathbf{x} + \mathbf{d} \\ \mathbf{g} = (\partial J/\partial \mathbf{x} \quad \partial J/\partial \mathbf{y})^T \end{cases}, \quad (16)$$

where  $\partial J/\partial \mathbf{x}$  and  $\partial J/\partial \mathbf{y}$  are the direction gradient values. After this operation, the displacement can be obtained. Finally, the stereo matching of speckle measurement can be achieved by combining the equations.

The experiment site diagrams are shown in Fig.5. A Swiwin's SW60B miniature turbojet engine was used. The SW60B turbojet engine was 84 mm in width, 203 mm in length, and 783 g in weight. The rotating speed was 50 000—160 000 rpm with a standard thrust 6 kg, and the rated exhaust temperature was 650 °C. The YIOU DP2000 anemometer was selected for the experiment. The measuring range was 0±3 000 Pa, the resolution was 1 Pa, the wind speed range was 1.00—100.00 m/s, and the wind speed resolution was 0.01 m/s. The pitot tube was made of YIOU brand LPT-06-200 Model L. The pitot tube was also made of 304 stainless steel. The gas velocity measuring range was 2—70 m/s and the pitot tube coefficient was between 0.99 and 1.01. The camera resolution was modified to be 1 920×1 080 pixels and the focus length was 1.9 mm. The distance between the camera and the center of the electric furnace was 478 mm, and the distance from the center of the electric furnace to the background grain image was 246 mm. The size of the background image was 210 mm×297 mm, and the number of the red, green, and blue dots (size 5 pixels) on the background image was 300 each, 900 in total. These dots were randomly generated by the computer. The industrial high-precision platinum-iridium thermocouple applied model type was WRP-130 S. The temperature measurement accuracy of the equipment was in the range of 0—1 600 °C, with an

error of  $\pm 1.5\text{ }^\circ\text{C}$ . The laboratory temperature condition was  $27\text{ }^\circ\text{C}$ , and the calculated environmental refractive index was 1.000 260. The pixel offset value of the background image could be perceived by taking photos.

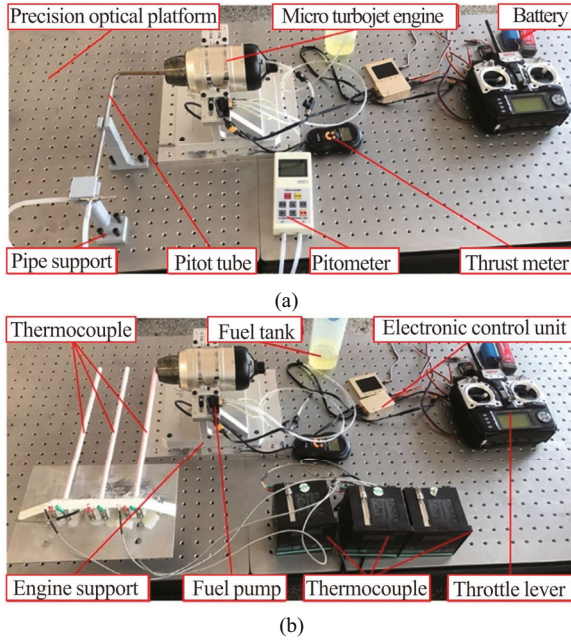


**Fig.5 The experiment site diagrams: (a) Pressure measure site diagram; (b) Temperature measure site diagram**

According to the size measurement of the tail nozzle of the actual turbojet engine, a simulation model of the calculation area was established. The calculation area included the extension section, the contraction section, the outer cylinder, the nozzle outer flow, and the tail flow, as shown in Fig.6.

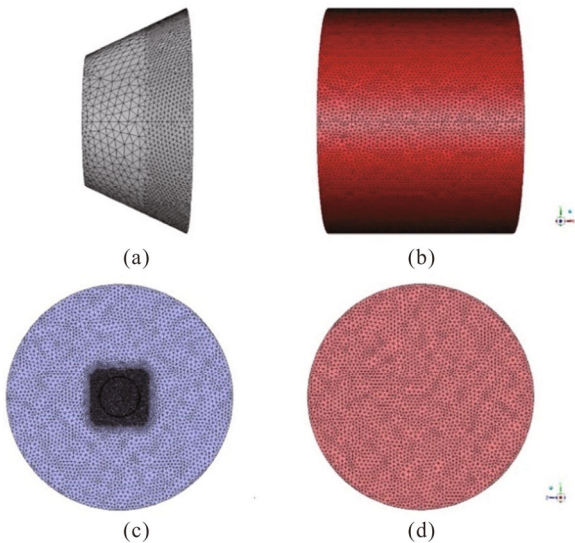


**Fig.6 Simulation conditions: (a) Exhaust nozzle; (b) Boundary of the atmospheric outflow; (c) Local mesh encryption; (d) Calculation domain exit**

The distance from the upper boundary to the nozzle was 4.5 times of the diameter of the nozzle outlet. The distance from the outlet boundary to the nozzle was 15 times of the diameter of the nozzle outlet. According to the grid-independent solution test, the optimal grid number was 1 000 000.

As shown in Fig.6, the calculation domain from the center to the periphery contained the nozzle inlet and the atmospheric outflow inlet, which provided the speed inlet boundary conditions. Fig.6(b) shows the boundary of the atmospheric outflow, which gave the far-field atmospheric pressure outlet boundary conditions. Fig.6(d) shows the calculation domain exit, which gave the far-field atmospheric pressure exit boundary. Moreover, the nozzle walls had non-slip, adiabatic boundary conditions.

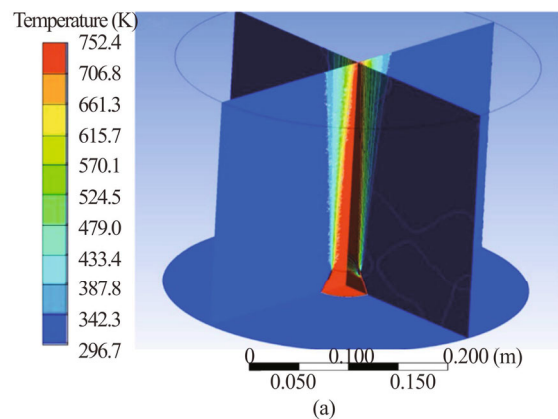
The temperature field simulation of the axisymmetric contraction and the expansion nozzle tail gas flow required that the Navier-Stokes equations of the compressible flow should be solved. These equations included the continuity equation (Eq.17), momentum equation (Eq.18), energy equation (Eq.19), etc.

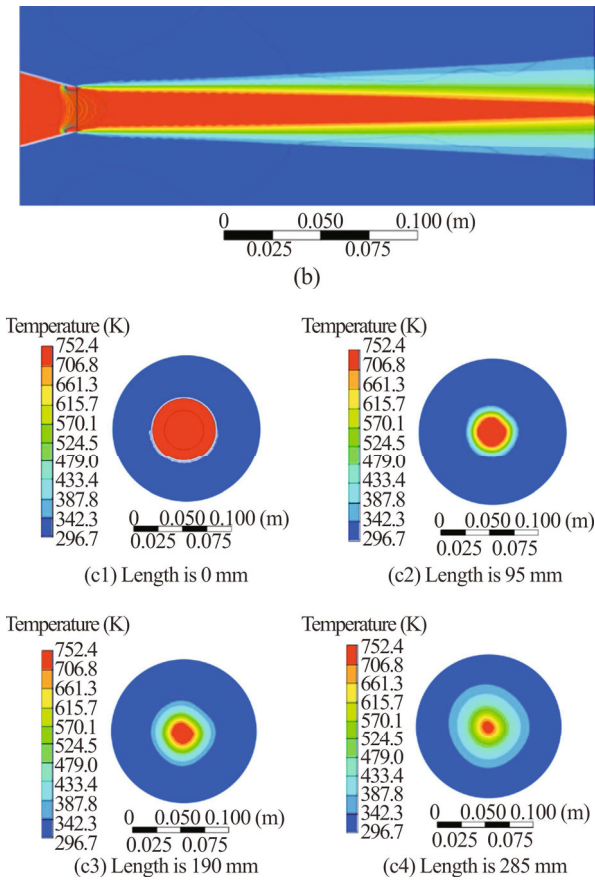
$$\frac{\partial(\rho u_j)}{\partial x_j} = 0, \tag{17}$$

$$\frac{\partial(\rho u_i u_j)}{\partial x_j} = -\frac{\partial p}{\partial x_i} + \mu \frac{\partial}{\partial x_i} \left( \frac{\partial u_i}{\partial x_i} + \frac{\partial u_j}{\partial x_j} - \frac{2\partial u_k \delta_y}{3\partial x_k} \right) + \rho f_i, \tag{18}$$

$$\frac{\partial}{\partial x_j} (\rho u_j H) = -\frac{\partial q_j}{\partial x_j} + \frac{\partial(\tau_{ij} u_j)}{\partial x_j} - \frac{\partial(J_{ij} h_i)}{\partial x_i} + S_a + \rho f_i u_i, \tag{19}$$

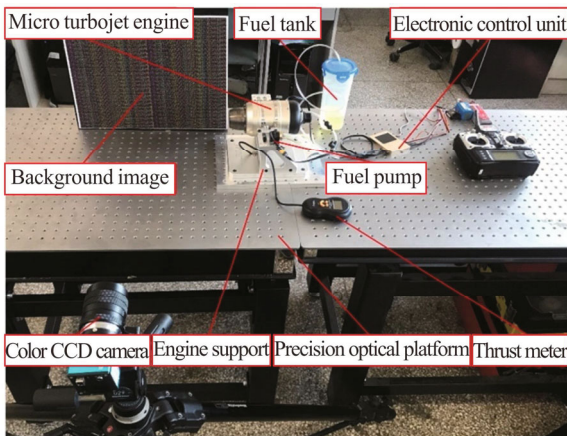
where  $\rho$  is the density of the fluid,  $u$  is the velocity of the fluid,  $p$  is the static pressure of the fluid,  $\mu$  is the dynamic viscosity coefficient of the fluid,  $\delta_{ij}$  is the Crocker's operator,  $h$  is the enthalpy,  $H$  is the total enthalpy,  $J_{ij}$  is the diffusion mass flux,  $S_a$  is the external heat source caused by the surface reaction, radiation, etc.,  $\tau_{ij}$  is the tensor of the viscosity,  $f_i$  is the volume force, and  $q_i$  is the heat flux. The closing of the equation applied the realizable  $k-\epsilon$  turbulence model. Additionally, the near-wall region was processed with the standard wall function method. Based on numerical simulation, the results are shown in Fig.7.





**Fig.7 Simulation results: (a) 3D temperature field; (b) Side view; (c) Cross section view**

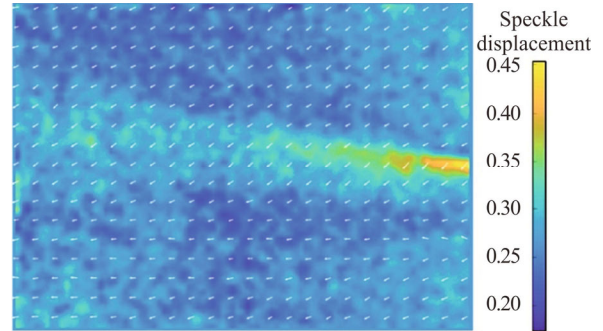
According to the relationship between the density field and the temperature in Eq.(8), the corresponding temperature gradient could be obtained. The three-dimensional temperature field was reconstructed using the BOS method. The experimental field map is shown in Fig.8.



**Fig.8 Field map of the experiment**

As the engine speed is adjusted to a steady running state, there are variations in the region of the temperature field at different speed operations.

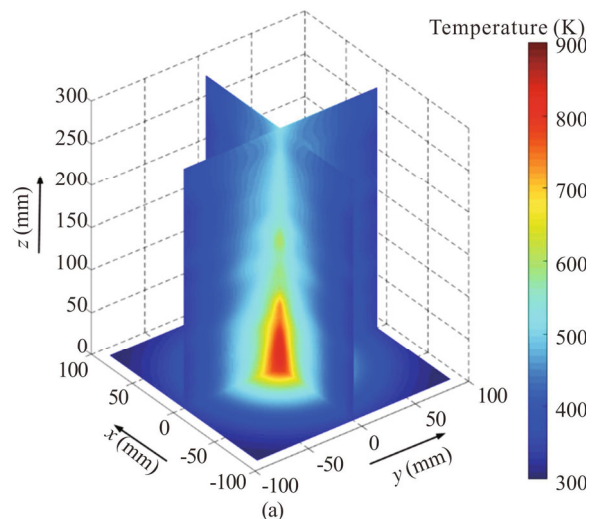
By comparing the background images before and after the engine ignition, the background speckle offset could be obtained, as shown in Fig.9.



**Fig.9 Background PIV measurement results**

The corresponding temperature gradient could be obtained from the relationship between the speckle move and temperature. To reconstruct the temperature field, the Abel inverse transformation was used to perform the iterative reconstruction of the section at the flame height of  $z=0$  mm in the  $x$ -direction. This process was repeated every 90 pixels on the  $z$ -direction. The result of the iteration is the temperature field in that scene. The calculations of the temperature field at different speed operations are shown in Fig.10.

Compared with the Ansys simulation results, the CBOS method was reliable and the accuracy was satisfactory. The measurement results of the platinum-iridium thermocouple were affected by the exhaust airflow inside the flame. The figure on the meter fluctuated in the range of 1%. Owing to the influence of the airflow, the temperature value of the thermocouple could be used as a reference for the entire temperature field. The comparison of the calculated data with the measured data of the thermocouple in different speed operating states is shown in Fig.11.



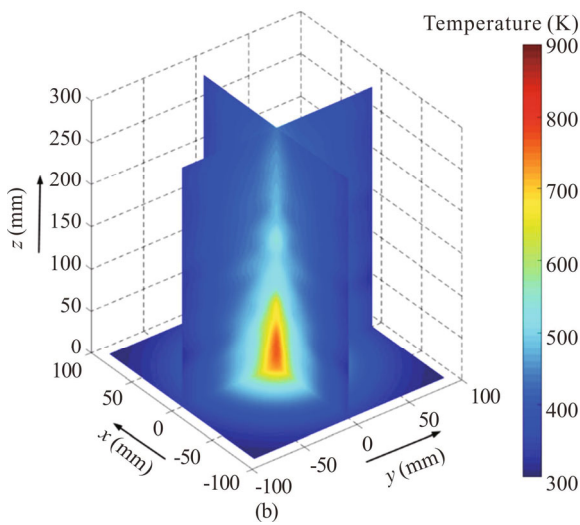


**Fig.10** Calculated temperature fields: (a) High-speed operation; (b) Low-speed operation

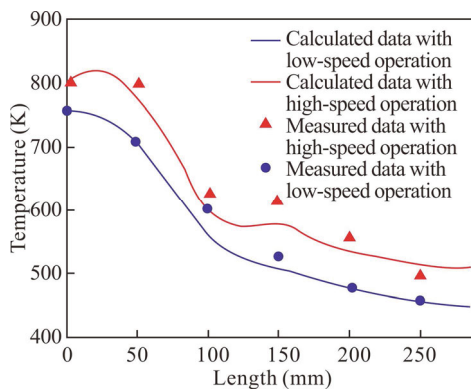


**Fig.11** Comparison between the calculated and measured data of the thermocouple in different speed operating states

Because there were many factors affecting the temperature, only the ideal air state was considered in the modelling and simulation, so the ANSYS simulation had some errors.

The tail jet temperature of the turbojet engine used in the laboratory is slightly lower than the engine tail gas temperature field used in civil airliners. The turbofan engine model pw4000 has a maximum tail jet temperature between 690 °C and 760 °C in the cruise stage and can reach up to 1 100 °C in the take-off phase stage<sup>[14,15]</sup>. The method in this paper is not influenced by the absolute temperature, but only by the temperature gradient. Higher actual engine tail flame temperatures will produce larger temperature gradients and thus more significant imaging biases. Therefore, the present method is an important guide for the measurement of the actual tail flame temperature field.

Compared to the temperature measured by the thermocouple, the calculated temperature drop trend near the nozzle was similar, and the error accuracy was about 10%.

The index of refraction was not only affected by temperature, but also by many other factors. Therefore, this research was focused on the relationship between the index of refraction and the temperature. We will further discuss the relationship between the index of refraction and other factors in the future in order to improve the temperature measurement accuracy.

In this research, the CBOS method was used to reconstruct the temperature field of aero engine exhaust. The temperature fields for aero engine exhaust were simulated with ANSYS method and FLUENT software. For the EGT field of the engine, the reconstructed results of CBOS were close to the simulation results for the numerical values. The application of CBOS for the engine exhaust could effectively reduce the measurement impact caused by the high-speed airflow of the engine exhaust. The advantage of this method was that there were relatively few restricted conditions. Because of the corresponding relationship between the temperature field and the refractive index, the reconstruction of the temperature field obtained using background Schlieren method was fast, and the real-time monitoring of the temperature field could then be realized. The effect of the 3D reconstruction of the engine exhaust temperature field with the method of CBOS was satisfactory. This method avoided some of the influencing factors in the measurement and appropriate precision was obtained for the aero engine exhausted temperature field.

### Statements and Declarations

The authors declare that there are no conflicts of interest related to this article.

### References

- [1] AMRUTHA K N, BHARATH Y K, JAYANTHI J. Aircraft engine fuel flow parameter prediction and health monitoring system[C]//2019 4th International Conference on Recent Trends on Electronics, Information, Communication & Technology (RTEICT), May 17-18, 2019, Bangalore, India. New York: IEEE, 2019: 39-44.
- [2] ZHONG S, LI Z, LIN L, et al. Aero-engine exhaust gas temperature prognostic model based on gated recurrent unit network[C]//2018 IEEE International Conference on Prognostics and Health Management (ICPHM), June 11-13, 2018, Seattle, WA, USA. New York: IEEE, 2018: 1-5.
- [3] GEORGE B, MUTHUVEERAPPAN N. Life assessment of a high temperature probe designed for performance evaluation and health monitoring of an aero gas turbine engine[J]. International journal of turbo & jet-engines, 2020: 000010151520200037.
- [4] ALLISON S W, GILLIES G T. Remote thermometry with thermographic phosphors: instrumentation and applications[J]. Review of scientific instruments, 1997,

- 68(7): 2615-2650.
- [5] MEIER G E A. New optical tools for fluid mechanics[J]. *Sadhana*, 1998, 23(5-6): 557-567.
- [6] VERSO L, LIBERZON A. Background oriented Schlieren in a density stratified fluid[J]. *Review of scientific instruments*, 2015, 86(10): 103705.
- [7] RAJSHEKHAR G, AMBROSINI D. Multi-scale approach for analyzing convective heat transfer flow in background-oriented Schlieren technique[J]. *Optics and lasers in engineering*, 2018, 110: 415-419.
- [8] LEE S, KIM S H, LEE H J, et al. Density acquisition and aero-optics measurement from BOS images for a hot jet[J]. *International journal of aeronautical and space sciences*, 2018, 19(3): 563-574.
- [9] LEOPOLD F, OTA M, KLATT D, et al. Reconstruction of the unsteady supersonic flow around a spike using the colored background oriented Schlieren technique[J]. *Journal of flow control measurement & visualization*, 2013, 01(2): 69-76.
- [10] SOURGEN F, LEOPOLD F, KLATT D. Reconstruction of the density field using the colored background oriented Schlieren technique (CBOS)[J]. *Optics and lasers in engineering*, 2012, 50(1): 29-38.
- [11] LEOPOLD F, OTA M, KLATT D, et al. Reconstruction of the unsteady supersonic flow around a spike using the colored background oriented Schlieren technique[J]. *Journal of flow control, measurement & visualization*, 2013, 1(2): 69-76.
- [12] RUBLEE E, RABAUD V, KONOLIGE K, et al. ORB: an efficient alternative to SIFT or SURF[C]//2011 International Conference on Computer Vision, November 6-13, 2011, Barcelona, Spain. New York: IEEE, 2011: 12491177.
- [13] DELPONTE E, ISGRO F, ODONE F, et al. SVD-matching using SIFT features[J]. *Graphical models*, 2005, 68(5-6): 415-431.
- [14] ZHANG H, DONG K. Prediction of aero-engine exhaust gas temperature based on autoregressive integrated moving average model[C]//2017 2nd International Conference on Automation, Mechanical Control and Computational Engineering (AMCCE 2017), March 25-26, 2017, Beijing, China. Paris: Atlantis Press, 2017: 477-480.
- [15] OETTINGER M, WEIN L, MIMIC D, et al. Automated detection of hot-gas path defects by support vector machine based analysis of exhaust density fields[J]. *Journal of the global power and propulsion society*, 2021, Special issue: data-driven modelling and high-fidelity simulations: 1-16.